

Dr. Francesc Viñes Solana  
*Departament de Ciència de Materials i  
Química Física*

Dr. Àngel Morales García  
*Departament de Ciència de Materials i  
Química Física*



# Treball Final de Grau

**Carbide MXenes Surface Tension Effect on CO<sub>2</sub> Capture**  
**Efecto de la tensión superficial de MXenos de carbono en la  
captura de CO<sub>2</sub>**

Daniel Dolz Garcia

*July 2020*



UNIVERSITAT DE  
BARCELONA

**B:KC** Barcelona  
Knowledge  
Campus  
Campus d'Excel·lència Internacional



Aquesta obra esta subjecta a la llicència de:  
Reconeixement–NoComercial–SenseObraDerivada



<http://creativecommons.org/licenses/by-nc-nd/3.0/es/>



*In the fields of observation chance favours only  
the prepared mind.*

*Louis Pasteur*

Este trabajo no se habría podido realizar sin la ayuda de Ángel y Fransis, magníficos tutores que me han apoyado todo y más, Oscar y Luis, por ese apoyo emocional en los momentos más complicados de este trabajo, David y Fileto por las tardes que nos hemos pasado compartiendo experiencias, errores y ayuda y sin mis padres y familia, que siempre han estado ahí. Gracias a todos por todo. Este no es sino el comienzo.



**REPORT**





# CONTENTS

<b>1. SUMMARY</b>	3
<b>2. RESUMEN</b>	5
<b>3. INTRODUCTION</b>	7
<b>4. OBJECTIVES</b>	9
<b>5. THEORETICAL BACKGROUND</b>	11
5.1. Quantum Chemistry	11
5.1.1. The Schrödinger Equation and Approximation Methods	11
5.1.2. Density Functional Theory	12
5.1.2.1. Exchange and Correlation Functionals	14
5.2. Bloch Theorem and Periodic Systems	14
5.3. Structures	14
5.4. Exfoliation Energy	16
<b>6. COMPUTATIONAL DETAILS</b>	17
<b>7. RESULTS AND DISCUSSION</b>	19
7.1. Reproducibility	19
7.2. Exfoliation Energy	20
7.3. Effect of the early transition metal	24
7.4. Effect of the <i>p</i> -block element	26
7.5. Width Effect	28
7.6. Bond distance M-A effect	29
<b>8. CONCLUSIONS</b>	31
<b>9. REFERENCES AND NOTES</b>	33
<b>APPENDICES</b>	35
Appendix 1: Tables	37
Appendix 2: Graphs	39



# 1. SUMMARY

One of the major challenges of our nowadays society is the fight against climate change derived from the gradual global warming of the Earth surface due to the high concentration of detrimental greenhouse gases in the atmosphere, such as CO<sub>2</sub> or CH<sub>4</sub>. These gases absorb the radiated heat emitted by the Earth toward space consequently promoting the so-called greenhouse effect. In principle, this effect is beneficial, because it leads to the thermal stability that is essential for life. However, the anthropogenic activity has derived into a great dependency of fossil fuels, especially since the industrial revolution, generating an excessive concentration of the above-mentioned gases, and so increasing the Earth temperature leading as well to the acidification of oceans. Nowadays, the CO<sub>2</sub> concentration in the atmosphere has reached 360 ppm, and this amount is expected to be doubled by the end of this century. The direct consequence of such concentration is the increase of the Earth's temperature, expected to rise 2-5 °C, leading to the melting of the poles, augmenting the level of the sea, and causing floods and other devastating phenomena across the world. To minimize, even avoid such consequences, new technologies are sought to reduce these greenhouse gases concentrations.

The usage of CO<sub>2</sub> sweeper derived materials emerges as a suitable technology for Carbon Capture and Storage (CCS). In this context, Transition Metal Carbides (TMCs) materials have been suggested as potential substrates for CO<sub>2</sub> capture and activation due to the exothermic CO<sub>2</sub> adsorption even at low partial pressures. Interestingly, the two-dimensional counterparts of TMCs, called MXenes, have shown an even better performance for CCS. These MXenes are synthesized by MAX phase precursors exfoliation techniques, thus depending on the MAX phases composition and demanding a certain energy to foster the layers separation. Indeed, such an exfoliation energy could be a descriptor to seize the resulting MXene chemical activity, here analyzed in depth through computational simulations, correlating the CO<sub>2</sub> adsorption energies on MXenes with the estimates of exfoliation energies.

**Keywords:** MAX Phases, MXenes, Density Functional Calculations, CO<sub>2</sub> capture, Environmental Science



## 2. RESUMEN

Uno de los principales desafíos de nuestra sociedad actual es la lucha contra el cambio climático derivado del calentamiento global gradual de la superficie de la Tierra debido a la alta concentración de gases de efecto invernadero perjudiciales en la atmósfera, como CO<sub>2</sub> o CH<sub>4</sub>. Estos gases absorben el calor irradiado emitido por la Tierra hacia el espacio, lo que promueve el llamado efecto invernadero. En principio, este efecto es beneficioso, ya que conduce a la estabilidad térmica que es esencial para la vida. Sin embargo, la humanidad ha desarrollado una gran dependencia por los combustibles fósiles, especialmente desde la revolución industrial, generando una concentración excesiva de los gases mencionados anteriormente, y aumentando así la temperatura de la Tierra y la acidificación de los océanos. Hoy en día, la concentración de CO<sub>2</sub> en la atmósfera ha alcanzado las 360 ppm, y se espera que esta cantidad se duplique para fines de este siglo. Esto llevará a un aumento de entre 2 a 5 grados centígrados de la temperatura global, que conducirá al derretimiento de los polos, aumento del nivel del mar e inundaciones y otros fenómenos devastadores. Para minimizar esto, se están buscando nuevas formas de reducir estas concentraciones de gases de efecto invernadero.

La captura y almacenamiento de carbono (*Carbon Capture Storage - CCS*) aparece como una tecnología adecuada para lograr este fin. Los carburos de metales de transición (*Transition Metal Carbides - TMC*) se han sugerido como sustratos potenciales para la captura y activación de CO<sub>2</sub> debido a su adsorción exotérmica de CO<sub>2</sub> incluso a bajas presiones parciales. Curiosamente, las contrapartes bidimensionales de TMC, llamadas MXenes, han mostrado un rendimiento aún mejor para CCS. Estos MXenes se sintetizan mediante técnicas de exfoliación de fases MAX precursoras, que dependen de la composición de las fases MAX y exige una cierta energía para fomentar la separación de las capas. De hecho, dicha energía de exfoliación podría ser un descriptor para aprovechar la actividad química resultante de MXene, aquí analizada en profundidad a través de simulaciones computacionales, correlacionando las energías de adsorción de CO<sub>2</sub> en MXenes con las estimaciones de las energías de exfoliación.

**Palabras clave:** Fases MAX, MXenes, Cálculos funcionales de densidad, captura de CO<sub>2</sub>, Ciencia ambiental



### 3. INTRODUCTION

One of the major challenges of our society is to provide an overall effective solution to climate change, which is leading damages that endanger our own livelihood. The climate change is a consequence of many factors, and among them, the global warming is the main actor. Global warming is related with the appearance of an abnormal high concentration of greenhouse gases, such as carbon dioxide (CO<sub>2</sub>) or methane mainly derived from anthropogenic activities. These gases act as heat-traps, which promote the greenhouse effect. Nowadays, the CO<sub>2</sub> concentration in the atmosphere has reached 360 ppm, and it is expected to continue increasing in the oncoming decades.<sup>1</sup> The consequences are dramatic, as Earth temperature is expected to rise 2-5 °C, thus unavoidably leading to the melting of the poles, with dramatic consequences such as provoking the increasing of the sea level, causing floods and other dangerous phenomena across the world,<sup>2</sup> unless actions are taken to reverse the present situation.

In the recent years society has recognized this critical situation, demanding urgent ecofriendly protocols to the nations with the ultimate goal of reducing the CO<sub>2</sub> emissions. Such actions require an energetic transition towards sustainable and novel energy sources based on renewable protocols, which would reduce the environmental impact. Not only the emissions have to be minimized; another challenge is the cleaning of the air by using appropriate sweep materials with a noted affinity towards greenhouse gases.<sup>3</sup> In the case of CO<sub>2</sub>, air Carbon Capture and Storage (CCS)<sup>4</sup> technologies are object of study for such a purpose.

In short, CCS techniques require the use of substrates with a notorious affinity for any of the greenhouse gases. In the case of CO<sub>2</sub> several materials have been tested, with poor success given its high chemical stability.<sup>5</sup> Fortunately, Transition Metal Carbides (TMCs) have been posed as potential candidates for CCS,<sup>6</sup> featuring a great CO<sub>2</sub> adsorption strength even at current atmospheric CO<sub>2</sub> content. More recently, two-dimensional counterparts of TMCs, so-called MXenes, have been confirmed to have an even better performance towards CCS,<sup>7</sup> and so have shown as well the nitride-based MXenes.<sup>8</sup>

Such MXenes are created by selective etching of a MAX precursor, composed by an early transition metal (M), a *p* block metal (A), and either carbon or nitrogen (X), with compositions of  $M_{n+1}AX_n$  and  $n = 1-3$ , see Figure 1.<sup>9</sup> This etching process is normally carried out using hydrofluoric acid,<sup>10,11</sup> yet there are other more novel fluorine-free protocols to selectively remove the A element.<sup>12</sup> Finally, the separation of the generated  $M_{n+1}X_n$  layers is carried out by ultrasounds.<sup>13</sup> At the end of the day, each MAX precursor has an exfoliation energy that depends on the strength of the M-A bonding. In principle, the reactivity (or stability) of the synthesized MXene could be connected to such an exfoliation energy. The hypothesis would imply that MXenes with high exfoliation energies would be less stable, and so more chemically active than those with a lower exfoliation energy.

1 <b>H</b> Hydrogen																	2 <b>He</b> Helium
3 <b>Li</b> Lithium	4 <b>Be</b> Beryllium											5 <b>B</b> Boron	6 <b>C</b> Carbon	7 <b>N</b> Nitrogen	8 <b>O</b> Oxygen	9 <b>F</b> Fluorine	10 <b>Ne</b> Neon
11 <b>Na</b> Sodium	12 <b>Mg</b> Magnesium											13 <b>Al</b> Aluminum	14 <b>Si</b> Silicon	15 <b>P</b> Phosphorus	16 <b>S</b> Sulfur	17 <b>Cl</b> Chlorine	18 <b>Ar</b> Argon
19 <b>K</b> Potassium	20 <b>Ca</b> Calcium	21 <b>Sc</b> Scandium	22 <b>Ti</b> Titanium	23 <b>V</b> Vanadium	24 <b>Cr</b> Chromium	25 <b>Mn</b> Manganese	26 <b>Fe</b> Iron	27 <b>Co</b> Cobalt	28 <b>Ni</b> Nickel	29 <b>Cu</b> Copper	30 <b>Zn</b> Zinc	31 <b>Ga</b> Gallium	32 <b>Ge</b> Germanium	33 <b>As</b> Arsenic	34 <b>Se</b> Selenium	35 <b>Br</b> Bromine	36 <b>Kr</b> Krypton
37 <b>Rb</b> Rubidium	38 <b>Sr</b> Strontium	39 <b>Y</b> Yttrium	40 <b>Zr</b> Zirconium	41 <b>Nb</b> Niobium	42 <b>Mo</b> Molybdenum	43 <b>Tc</b> Technetium	44 <b>Ru</b> Ruthenium	45 <b>Rh</b> Rhodium	46 <b>Pd</b> Palladium	47 <b>Ag</b> Silver	48 <b>Cd</b> Cadmium	49 <b>In</b> Indium	50 <b>Sn</b> Tin	51 <b>Sb</b> Antimony	52 <b>Te</b> Tellurium	53 <b>I</b> Iodine	54 <b>Xe</b> Xenon
55 <b>Cs</b> Cesium	56 <b>Ba</b> Barium	57-71	72 <b>Hf</b> Hafnium	73 <b>Ta</b> Tantalum	74 <b>W</b> Tungsten	75 <b>Re</b> Rhenium	76 <b>Os</b> Osmium	77 <b>Ir</b> Iridium	78 <b>Pt</b> Platinum	79 <b>Au</b> Gold	80 <b>Hg</b> Mercury	81 <b>Tl</b> Thallium	82 <b>Pb</b> Lead	83 <b>Bi</b> Bismuth	84 <b>Po</b> Polonium	85 <b>At</b> Astatine	86 <b>Rn</b> Radon
87 <b>Fr</b> Francium	88 <b>Ra</b> Radium	89-103	104 <b>Rf</b> Rutherfordium	105 <b>Db</b> Dubnium	106 <b>Sg</b> Seaborgium	107 <b>Bh</b> Bohrium	108 <b>Hs</b> Hassium	109 <b>Mt</b> Meitnerium	110 <b>Ds</b> Darmstadtium	111 <b>Rg</b> Roentgenium	112 <b>Uum</b> Ununbium	113 <b>Uut</b> Ununtrium	114 <b>Uuq</b> Ununquadium	115 <b>Uup</b> Ununpentium	116 <b>Uuh</b> Ununhexium		

Figure 1: The marked elements compose the usual MAX phases. Early transition metals (M), p-block-elements (A) and carbon/nitrogen (X) are highlighted in blue, yellow, and green, respectively.

Following this premise and given the great capability of MXenes for trapping  $\text{CO}_2$ , the main goal of this project is to investigate whether the exfoliation energies, regarded as a sort of surface tension, required to generate MXene phases correlate with adsorption energies of the  $\text{CO}_2$  molecule. To this end, a thorough computational study comprising a total of 486 MAX and MXenes phases, with  $M_{n+1}AX_n$  and  $M_{n+1}X_n$  ( $n=1-3$ ) stoichiometries, respectively, have been analyzed by Density Functional Theory (DFT) means.



## 4. OBJECTIVES

The main objective of this research project is to investigate the possible influence of MAX exfoliation energy over the capacity of the generated MXene phase to adsorb CO<sub>2</sub>. To shed light on this goal, the following particular questions will be addressed:

- What is the influence of the MAX phase M and X composition and  $n$  thickness on the resulting exfoliation energy?
- What is the influence of the A phase on the exfoliation energy of the MAX phases given a particular composition?
- Is it feasible to establish a tentative correlation between MAX structural parameters such as atomic distances (e.g. M-A) and exfoliation energies?
- Are there any differences between carbide or nitride derived MXenes?



## 5. THEORETICAL BACKGROUND

### 5.1. QUANTUM CHEMISTRY

Classical mechanics established the laws of the macroscopic world related to the movement of objects. However, such classical laws fail in the nanoscale, where the system atomic size plays a fundamental role. Here, quantum mechanics lay down the laws to properly describe the properties of the matter. One branch is quantum chemistry, which studies the properties of chemical systems composed from a single to a number of atoms. The knowledge of the total energy of these systems, obtained by solving the Schrödinger equation, allows one to assess the systems stability, and other properties can be gained when knowing the system wave function. Thus, quantum chemistry can be used not only to the study of well-established systems, but to discover new materials without experimental evidence.

#### 5.1.1. The Schrödinger Equation and Application Methods

The energy of a particular system is accessible to by solving the time independent Schrödinger equation,<sup>14</sup> which gives information about stationary states:

$$\hat{H}\Psi_o = E_o\Psi_o \quad (\text{Eq. 1}),$$

where  $\hat{H}$  is the Hamiltonian operator,  $\Psi_o$  is the many-electron wave function, and  $E_o$  is the ground state system energy.  $\hat{H}$  is defined as the contribution of different energetic terms:

$$\hat{H} = \hat{T}_e + \hat{T}_n + \hat{V}_{ee} + \hat{V}_{en} + \hat{V}_{nn} \quad (\text{Eq. 2}),$$

where  $\hat{T}_e$  and  $\hat{T}_n$  are the kinetic terms of electrons and nuclei, respectively. On the other hand,  $\hat{V}_{ee}$ ,  $\hat{V}_{en}$ , and  $\hat{V}_{nn}$  terms correspond to the electron-electron, electron-nuclei, and nuclei-nuclei

coulombic interactions, respectively. This expression, however, is practically unsolvable, demanding a simplification to make it feasible. To solve this, different approximation methods were implemented, starting with the Born-Oppenheimer Approximation (*BOA*).<sup>15</sup> Such approach is based on the difference of the kinetic energy of electrons and nuclei. The latter can be regarded as zero due to the mass of the electrons being much lower than the mass of the nuclei, so nuclei can be described as stationary points. Under this motion and decoupling the different terms, Schrödinger equation is reduced to solving the electronic contribution of  $\hat{H}_e$ :

$$\hat{H}_e = \hat{T}_e + \hat{V}_{ee} + \hat{V}_{en} \quad (\text{Eq. 3}).$$

Two main approximations are broadly used to solve the interaction between electrons in polyelectronic systems following a variational principle, the Hartree-Fock method (*HF*)<sup>16</sup> and the Density Functional Theory (*DFT*).<sup>17</sup> In the former approach, the N-electron wave function is treated as a single Slater determinant to approximate the wavefunction. These methods, generally referred to as wavefunctions based methods, can be rather exact yet computationally demanding. Consequently, alternative methods are sought, such as DFT, which relies in knowing only the electron density function.

### 5.1.2. Density Functional Theory

The DFT was developed by Kohn and Hohenberg in 1964 and based on the approach first considered in 1920 described as the Thomas-Fermi method.<sup>18,19</sup> It is based on defining the energy of a system as a functional—a function of a function—of the electron density,  $\rho(r)$ , *i.e.*  $E[\rho(r)]$ . This density thus determines the properties of the system yet must fulfill the following conditions:

$$\int \rho(r) dr = N \quad (\text{Eq. 4}),$$

$$\rho(r \rightarrow \infty) = 0 \quad (\text{Eq. 5}).$$

These two equations tell us that the integration of the electron density gives the total number of electrons,  $N$ , and the density value decays to zero at infinite distance. The  $\rho(r)$

determines  $N$ , through a given external potential  $V_{ext}(r)$ . So, one can now write the total energy of the system as:

$$E[\rho] = T[\rho] + E_{Ne}[\rho] + E_{ee}[\rho] = \int \rho(r)V_{Ne}(r)dr + F_{HK}[\rho] \quad (\text{Eq. 6}),$$

$$F_{HK}[\rho] = T[\rho] + E_{ee}[\rho] \quad (\text{Eq. 7}).$$

This formalism greatly simplifies the calculations, making the study of large systems composed by hundreds of atoms feasible, as the approach aims finding the energy of the ground state. This energy can only be when the functional  $F_{HK}[\rho]$  is the correct one, as only the one using the true ground state density delivers the lowest energy.<sup>20</sup> This makes the solution nothing but a variational principle type one:

$$E_o \leq E[\rho] = T[\rho] + E_{Ne}[\rho] + E_{ee}[\rho] \quad (\text{Eq. 8}).$$

The last part of the functional, the  $F_{HK}[\rho]$  term, is the tricky one, though. It contains the kinetic energy and the electron-electron interaction functionals, difficult to solve.<sup>21</sup>

Walter Kohn and Lu Jeu Sham proposed a fictitious system, named the Kohn-Sham system, with the same density as the real one, but where electrons do not interact.<sup>22</sup> Assuming this fictional system, the energy of the system can be expressed as follows:

$$E_o = T_s + E_{ext} + J + E_{xc} \quad (\text{Eq. 9}),$$

where  $T_s$  corresponds to the kinetic energy of the electrons,  $E_{ext}$  to the attraction between the electronic density and the external potential,  $J$  to the coulomb repulsion, and  $E_{xc}$  is a term that includes the rest of the interactions, mainly the difference in kinetic energy between the real system and the KS system, plus the correlation and exchange energies.

### 5.1.2.1 Exchange and Correlation Functionals

Now, the problematic aspect has been isolated in the exchange correlation term,  $E_{xc}$ . If this term would be known, the DFT framework would be exact. For now, this is nothing more than a wishful thinking, and the strategy to resolve this term passes through the development of approximations of increasing complexity and accuracy.<sup>23</sup> These improvements, however, can be quite computationally demanding, and so, could turn out to be not very useful.<sup>24</sup>

The most basic and simple approach was the Local Density Approximation (*LDA*), based on the assumption that the electron density does not much differ with the position.<sup>25</sup> Another improved one is the Generalized Gradient Approximation (*GGA*), which includes the density gradient in its calculations as a variable.<sup>26</sup> The evolution of this latter one is the so-called meta-GGA, that also considers the second derivative of the electron density function.<sup>27</sup> Other higher rungs exist, which add portions of HF exchange energy, or even tackle the exact energy, but at a high computational toll. In this study a GGA exchange-correlation functional is used, as is a best compromise in between accuracy and computational cost.

## 5.2. BLOCH THEOREM AND PERIODIC SYSTEMS

One of the advantages of working with extended materials is that the computational cost is significantly reduced making use of the intrinsic property of periodicity.<sup>28</sup> Bloch theorem is based on the principle that a single wavefunction that describes an electronic state must be periodic.<sup>29</sup> This enables the use of an unit cell to describe the properties of an infinite system. A peculiarity of this theorem is that the system described by this wavefunction is not defined in the real space, but in its reciprocal one. Both spaces are orthogonally connected, meaning that a short distance in the real lattice corresponds to a long one in the reciprocal space, and *vice versa*.<sup>30</sup>

## 5.3. STRUCTURES

Three-dimensional solids tend to feature a well-defined periodic structure. The simplest and basic reduction that leads to the formation of an extended solid by repeating itself is the so-called unit cell, defined by three vectors and three angles. The replication of such a unit cell along the three-dimensional space generates the desired material. Additional concerns have to be considered for designing surfaces and two-dimensional materials. In these cases, only two of the three possible directions offer periodicity, while the third one features the vacuum. Under

three-dimensional coordinates, a vector is defined, but a vacuum is required to avoid interaction between material replicas. Normally 10 Å is usually enough to minimize this interaction.

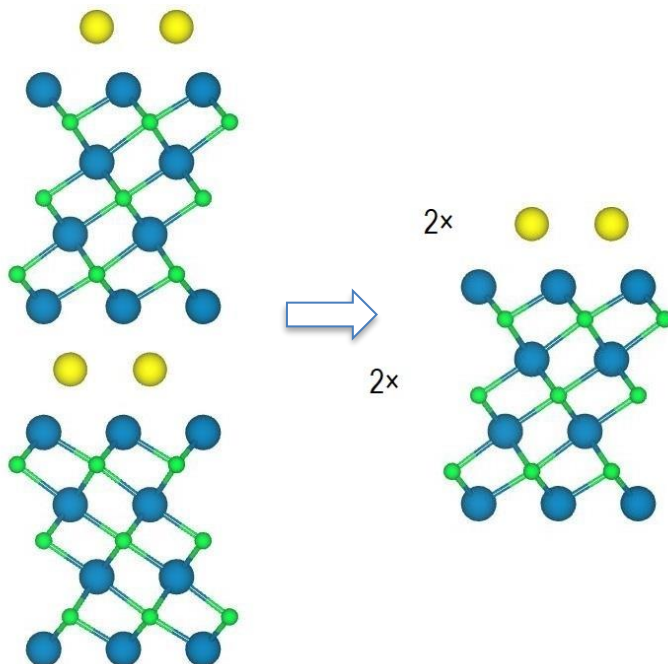


Figure 2: Exfoliation process for a MAX phase composed of layers of A element, shown as yellow spheres, gluing  $M_nX_3$  MXenes, where M and X elements are shown as blue and green spheres, respectively.

MAX phases are three-dimensional carbide or nitride compounds formed by a transition metal (M), an element of the  $p$  block (A), and X being C or N, with a stoichiometry of  $M_{n+1}AX_n$  and a certain width defined by  $n$ , ranging 1-3,<sup>31</sup> yet MAX phases with larger  $n$  have been discovered.<sup>32</sup> The MAX structure can be described as a layer of the A element separating what would later be the MXene after exfoliation, see Figure 2. These two-dimensional materials are isolated by the chemical etching of the MAX precursor using hydrofluoric acid (HF), followed by a sonication process to separate the MXene layers (see Figure 3), yet novel methods not requiring the use of HF have been developed.<sup>33,34</sup> Their structure is described as  $M_{n+1}X_n$  depending on the individual precursors.

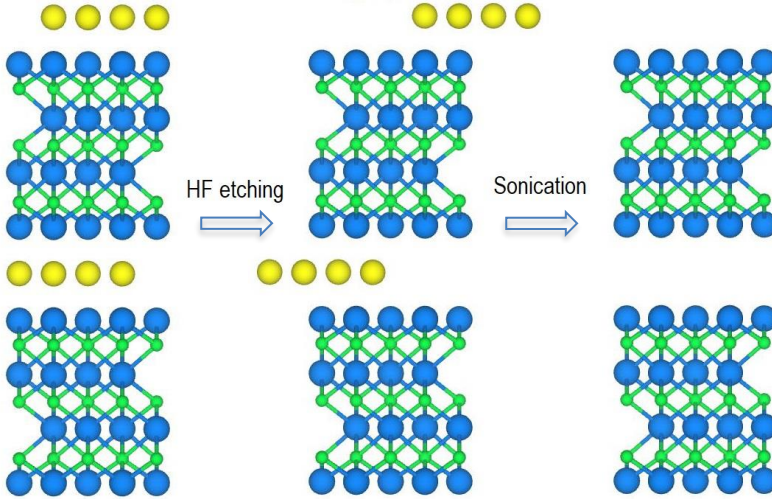


Figure 3: A schematic view on the etching and delaminating process by sonication.

## 5.4. EXFOLIATION ENERGY

The exfoliation energy of a solid can be understood as the energy required to disassemble an extended surface along one particular direction attending to chemical aspects such as the bonding weakness. As such, it is a form of surface tension. This energetic parameter is particularly interesting in layered materials, where the exfoliation energy (or interlayer binding energy) is used as a measurement of the feasibility to form sheets from the corresponding bulk layered material using a top-down synthesis protocol.<sup>35</sup> Attending to the MAX structure (see Figure 2), after exfoliating it, four phases are obtained corresponding to the two decoupled A layers and two isolated MXenes. Considering the surface area  $S$  of the MAX phase, we define thus the exfoliation energy,  $E_{exf}$  as follows:

$$E_{exf} = -[E_{MAX} - 2E_{MXene} - 2E_A]/(4S) \quad (\text{Eq. 10}),$$

In this case, being the MAX or MXene unit cell a hexagonal type, the surface is equal to  $\sqrt{3}a^2/2$ , being  $a$  the lattice parameter of the MAX or MXene phase.



## 6. COMPUTATIONAL DETAILS

In order to investigate the exfoliation energy needed to form MXenes from MAX precursors, first-principles periodic DFT based calculation are carried out on MAX bulk and MXene surface models. In particular, several MAX and MXene phases with  $M_{n+1}AX_n$  and  $M_{n+1}X_n$  respective stoichiometries — $M = \text{Ti, V, Cr, Zr, Nb, Mo, Hf, Ta, W}$ ;  $A = \text{Al, Si, P, Ga, Ge, As, In, Sn, Sb}$ ;  $X = \text{C, N}$ — with  $n = 1-3$  have been investigated. In addition, the A phase reference has been investigated considering either *i*) the resulting A layer immediately after exfoliation, *ii*) a single A atom in vacuum, or *iii*) the bulk phase of A, from which the energy of a single atom is calculated.

All calculations were performed under the GGA employing the Perdew-Burke-Ernzerhof (PBE)<sup>36</sup> exchange-correlation functional as implemented in the Vienna *Ab-initio* Simulation Package (VASP).<sup>37</sup> To describe the core interaction Projector Augmented Wave (PAW) potentials were used with a plane wave cutoff energy of 415 eV.<sup>38</sup> Numerical integrations in reciprocal space were carried out using optimal Monkhorst-Pack grids of  $9 \times 9 \times 9$ ,  $5 \times 5 \times 1$ , and  $1 \times 1 \times 1$  — $\Gamma$  point— dimensions for special  $\mathbf{k}$ -points for bulk, surfaces, and single atom models, respectively.<sup>39</sup> The geometry optimizations were considered converged when the forces acting on the nuclei were all below  $0.01 \text{ eV} \cdot \text{\AA}^{-1}$ .

The first set of studied MXenes were carbon-based MXenes, also called MCenes. Since the MCene cell vectors that come from a MAX phase are virtually the same, it would mean that no differences are observed when the A layer of the MAX phase changes. All energies of the MCenes were calculated accounting for different A layer dimensions, to observe whether there exists any change. Due to using different starting lattice parameters, final geometries differ a little, yet the final energy of the phases is roughly the same. Nitrogen-based MXenes, *a.k.a.* MNenes, were calculated the same way. Finally, we would like to point out that the nearly 1000 calculations were carried out in the computing cluster of the Institute of Theoretical and Computational Chemistry (IQTC) of the University of Barcelona.



## 7. RESULTS AND DISCUSSION

In this section, we shall discuss the obtained results, acquired with the aim of answering the aforementioned objectives. We will firstly start with the analysis of previous studies so as to ensure the suitability and reproducibility of our computational setup. Next, the exfoliation energies are discussed as a function of the MXene thickness. At this point, the plausible correlation between exfoliation energy and the adsorption of CO<sub>2</sub> on MXenes will be explored. This analysis will allow identifying trends as a function of the A element that composes the MAX phase. In addition, the M–A distance will be analyzed to investigate suitable correlation with the exfoliation energy. We would like to stress out that the study was initially proposed for just carbide-derived MXene materials, but with a working effort, we were able to extend it to nitride-derived ones.

### 7.1. REPRODUCIBILITY

First, we will compare our predictions with those previously reported in the literature by Khazaei *et al.*<sup>11</sup> As aforementioned, three different models are used to obtain the energy of  $E_A$ , including *i*) the energy of a single A atom placed in a large box, *ii*) the energy of A subtracted from the A separated sheet layer, and *iii*) the energy of A subtracted from the most stable bulk A phase. According to this, we obtained three different  $E_{\text{exf}}$  that are used to compare with the previous results.<sup>11</sup> Towards this purpose, we selected a set of 16 MAX phases including Hf<sub>2</sub>AlC, Hf<sub>2</sub>InC, Ti<sub>3</sub>AlC<sub>2</sub>, Ti<sub>4</sub>GeC<sub>3</sub>, V<sub>2</sub>GaC, V<sub>2</sub>SiC, V<sub>3</sub>AlC<sub>2</sub>, Zr<sub>2</sub>InC, Zr<sub>2</sub>SnC, Zr<sub>3</sub>AlC<sub>2</sub>, Nb<sub>2</sub>SnC, Nb<sub>2</sub>GaC, Nb<sub>2</sub>AsC, Nb<sub>2</sub>InC, Nb<sub>3</sub>SiC<sub>2</sub>, and Nb<sub>4</sub>AlC<sub>3</sub> allowing a comparison of results.

Figure 4 shows three different trends for each A reference compared to previous results. The best correlation is reported when  $E_A$  is taken from the most stable bulk A phase supported by a linear regression coefficient  $R$  of 0.99, as expected, since that was used in the previous work.<sup>11</sup> On the other hand, we have the worst correlation corresponding to the directly exfoliated phases, showing an  $R$  of 0.75. Finally, the intermediate situation is found when using the A in the vacuum as reference, with an  $R$  of 0.79. Considering the best correlation, we have

successfully reproduced of our results, plus we show here that exfoliation energies get more disperse, and generally higher, when one uses less condensed, or reduced dimensionality references; *i.e.* the lowest  $E_{\text{exf}}$  are found for three-dimensional bulk A, whereas the use of two-dimensional atomic sheets provides higher values, while highest being zero-dimensionality single atoms in vacuum. In any case, note that the differences observed between both studies are mainly due to computational details derived from the convergence criteria. For consistency, from here on, the  $E_{\text{exf}}$  values are discussed using bulk A as reference. These bulks have been computed using a  $9 \times 9 \times 9$  grid and doing a previous research to know the crystal structure of each of the elements. The majority presented a cubic crystal system, but there also were a few trigonal (As, In, Sb), orthorhombic (Ga), and triclinic (P).

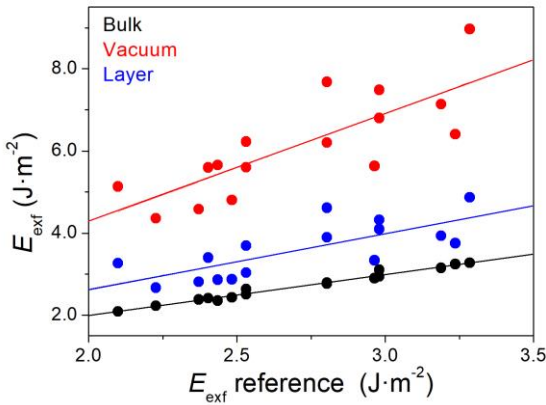


Figure 4: Comparison between calculated and reference  $E_{\text{exf}}$  values, where presently computed  $E_A$  of the  $p$ -block element have been acquired from three different references, bulk, sheet, or an atom in vacuum.

## 7.2. EXFOLIATION ENERGY

In this section, the variation of  $E_{\text{exf}}$  with respect the composition of the MAX phase based on  $M$ ,  $A$ , and  $X$  elements is discussed in detail. Table 1 lists the exfoliation energies of all MAX carbides and nitrides with  $M_2AX$  stoichiometry. Analogous results are obtained for  $M_3AX_2$  and  $M_4AX_3$  systems, compiled in Appendix 1. In general, the exfoliation energies in Table 1 for MAX derived carbides are systematically higher than their analogous derived nitrides.

		$E_{\text{exf}} \text{M}_2\text{AX} \text{ (J}\cdot\text{m}^{-2}\text{)}$									
<b>X</b>	<b>MA</b>	<b>Al</b>	<b>Si</b>	<b>P</b>	<b>Ga</b>	<b>Ge</b>	<b>As</b>	<b>In</b>	<b>Sn</b>	<b>Sb</b>	
<b>C</b>	<b>d<sup>2</sup></b>	<b>Ti</b>	2.76	3.16	3.64	2.96	3.17	3.24	2.55	2.68	2.47
		<b>Zr</b>	2.07	2.48	3.28	2.39	2.64	2.96	2.26	2.53	2.45
		<b>Hf</b>	2.36	2.74	3.53	2.64	2.82	3.08	2.40	2.60	2.44
	<b>d<sup>3</sup></b>	<b>V</b>	3.28	3.25	3.62	3.24	2.96	2.95	2.37	2.18	1.97
		<b>Nb</b>	2.87	2.85	3.45	2.92	2.74	2.95	2.48	2.37	2.20
		<b>Ta</b>	3.01	2.82	3.43	2.93	2.61	2.79	2.39	2.13	1.86
	<b>d<sup>4</sup></b>	<b>Cr</b>	3.45	3.19	3.11	3.14	2.76	2.53	2.10	1.92	1.68
		<b>Mo</b>	3.22	2.87	2.85	2.96	2.66	2.47	2.34	2.23	1.99
		<b>W</b>	3.43	2.90	3.08	3.03	2.58	2.26	2.37	2.07	1.75
<b>N</b>	<b>d<sup>2</sup></b>	<b>Ti</b>	3.09	3.27	3.72	3.17	3.08	3.12	2.44	2.31	2.16
		<b>Zr</b>	2.39	2.60	3.45	2.56	2.61	2.98	2.18	2.28	2.15
		<b>Hf</b>	2.61	2.69	3.54	2.71	2.63	2.93	2.20	2.15	1.91
	<b>d<sup>3</sup></b>	<b>V</b>	3.33	3.01	3.25	3.01	2.69	2.61	2.05	1.86	1.63
		<b>Nb</b>	3.43	2.71	3.25	3.11	2.56	2.69	2.21	2.12	1.96
		<b>Ta</b>	3.51	2.55	3.35	3.12	2.31	2.36	1.97	1.71	1.47
	<b>d<sup>4</sup></b>	<b>Cr</b>	3.20	3.00	2.79	2.90	2.55	2.31	1.94	1.81	1.54
		<b>Mo</b>	3.40	2.77	3.04	2.98	2.20	2.29	1.91	1.88	1.63
		<b>W</b>	3.28	2.44	2.55	2.71	1.83	1.62	1.14	1.01	0.77

Table 1: Exfoliation energies for carbide- and nitride-derived MXenes from a M<sub>2</sub>AX phase

The acquired information easily permits to know which MAX phase is preferred to get a certain MXene in terms of energy. For instance, when one wants to obtain the Ti<sub>2</sub>C MXene, the Ti<sub>2</sub>SbC MAX precursor is energetically the most favorable phase requiring only 2.47 J·m<sup>-2</sup>. In short, the *p*-block element which forms the MXene with the lowest exfoliation energy corresponds to Sb-derived MAX phases. This result constitutes a bias, because such low

exfoliation energy can also be attributed to unstable MAX phases. In particular, it is known that Sb phases are ones not energetically stable.<sup>40</sup> As an example, when one calculates the exfoliation energy for the  $W_4SbN_3$  MAX phase with Sb as a bulk, this energy is negative, which is probably a corollary of this phenomenon.<sup>40</sup> Clearly, exfoliation energies have to be screened based on MAX stability terms.

On the application field, MXenes have been recently shown to feature a great capability for trapping  $CO_2$ . Not surprisingly, the activation of  $CO_2$  depends on the MXene composition. Therefore, one can think that it is suitable to find correlation between the exfoliation energies and  $CO_2$  adsorption energies, implying that those MXenes with higher exfoliation energies, and so, being more unstable, would feature a higher chemical activity, and so, would be able to anchor the  $CO_2$  stronger as previously reported. Figure 5 below shows the trends of carbide MAX phases on the adsorption energies of  $CO_2$ , gained from previous works<sup>41</sup>—except for Cr-based MXenes, that were not earlier computed—, while the trends found in carbides are mostly maintained for nitrides, see Appendix 2. As one can clearly see, in general, the adsorption energies increase (becomes more negative) as the exfoliation energy increases, validating the hypothesis, and signaling  $E_{exf}$  as a possible physicochemical descriptor.

It seems as well that the correlation is maintained across groups and  $d$  series. For instance, Hf-, Zr-, and Ti-derived carbides expose the largest adsorption energies compared to the rest of MXenes, regardless of the MAX precursor. Between them, however, they follow the same trend, as  $E_{ads}$  is larger the greater  $E_{exf}$  is. Still, particularly Group IV MXenes can be treated differently. If one starts from Al, it can be seen that two different linear adjustments can be made: one for Zr, Hf, and Ti and another one with the rest of the elements. This trend is, however, lost as one advances along the  $d$  series, when all energies seem to converge in a single linear fit. It should be noted that Al-based MAX phases with Ti, Zr, and Hf seem to have very low exfoliation energies compared to the rest of phases while presenting at the same time very high  $CO_2$  affinities. This would mean that the preferred  $A$  element to exfoliate such MXenes would be Al, which, in accordance, tends to be the typical one in the so far explored MAX phases.<sup>9</sup> This feature is not so exacerbated in the case of nitride-based MXenes, as one can clearly see in Appendix 2.

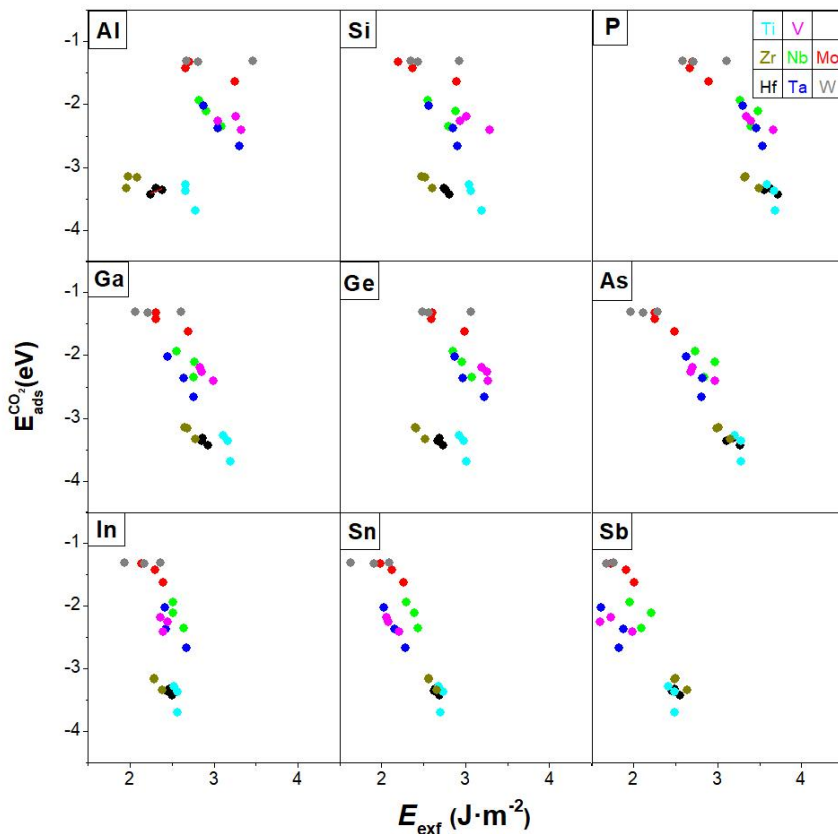


Figure 5: Trends for CO<sub>2</sub> adsorption energies as a function of the  $E_{\text{ext}}$  for  $M_{n+1}AX_n$  ( $n = 1-3$ ) phases

Notice that these values for adsorption energies are the ones used in the most stable adsorption site, *i.e.* the site with the most negative adsorption energy. Thus, one could argue that one is mixing different adsorption conformations, and such an effect bias the trends. To inspect that, several graphs for different adsorption sites have been plotted, leaving to the conclusion that there is no major difference on which adsorption conformation and sites are used. For instance, in Figure 6 we can see that the two trends are still easily visible in Al-based MAX phases.

Next, we focus on the contribution effect of the early transition metal  $M$  and the metal of the  $p$ -block,  $A$ , separately. As trends are independent from thickness, the focus will be placed on  $M_2AC$  phases.

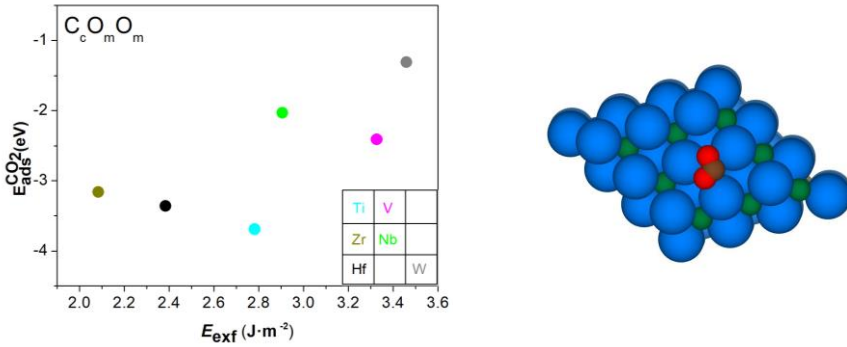


Figure 6: The same trends are present regardless of the adsorption site studied. The  $C_cO_mO_m$  adsorption site is shown to the right, seen from above. In this site, the  $CO_2$  molecule is adsorbed in a plane parallel to the surface. Blue, green, brown and red denote M, X, C and O, respectively. As seen in the graph, it presents the same trends found in the most stable adsorption site.

### 7.3. EFFECT OF THE EARLY TRANSITION METAL

For a better understanding, we shall start the discussion on the effect that  $M$  element induces on exfoliation energies. Figure 7 shows the variation of  $E_{\text{exf}}$  along the 3d Ti, V, and Cr series.

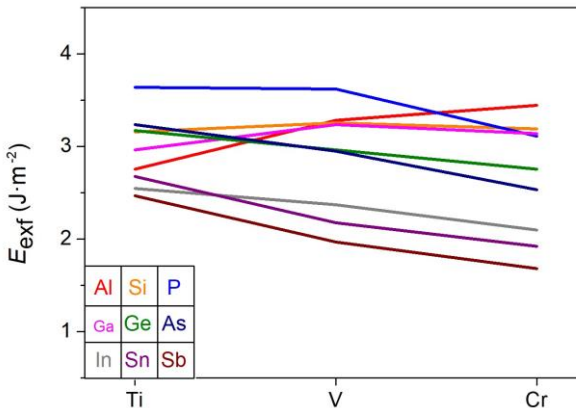


Figure 7:  $E_{\text{exf}}$  variations of Ti, V, and Cr-based  $M_2AC$  phases



In general, the  $E_{\text{exf}}$  goes down along the  $d$  series with the exception of Al-, Si- and Ga-derived MAX phases, where it increases. A similar comparison is performed along the Zr, Nb, and Mo  $4d$  series and very similar trends are observed, see Appendix 2. The formation of Hf-derived MXenes requires large  $E_{\text{exf}}$ , whereas W-derived ones requires the lowest  $E_{\text{exf}}$  regardless the A-layer, except for Al-derived MAX phases. Finally, along the Hf, Ta, and W  $5d$  series, see Appendix 2, values may increase/decrease, but for Al-, Si- and Ga-derived MAX phases,  $E_{\text{exf}}$  increases while decreases for the rest. In short, it can be easily seen that Al-, Si-, and Ga-derived MAX phases expose a positive trend of  $E_{\text{exf}}$  increasing the value when goes down in the early transition metal group, whereas  $E_{\text{exf}}$  increases its value in the As-, In-, Sn-, and Sb-derived MAX phases in the same direction.

Now, we shall analyze the trends along groups. Thus, for group IV, this is, Ti, Zr, and Hf, see Figure 8, a trend is found,  $E_{\text{exf}}$  decreases from Ti to Zr decreases, but increases back when going to Hf.

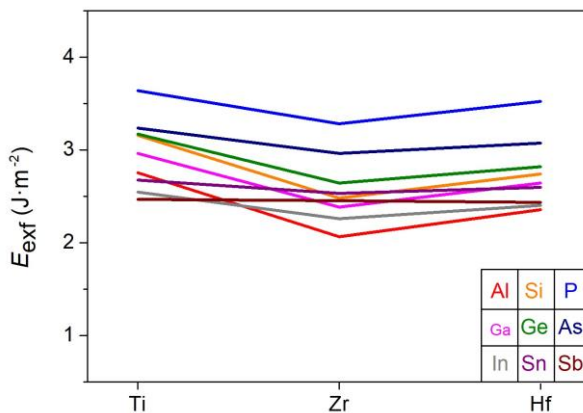


Figure 8:  $E_{\text{exf}}$  variations for Ti, Zr, and Hf-based  $M_2AC$  phases

This particular trend is not observed for group V, that is, V, Nb, Ta, see Figure 9. In this group, the energy decreases between V and Nb, but remains almost constant when moving forward. This changes though for In, Sn, and Sb, as they feature an increase/decrease in the  $E_{\text{exf}}$ .

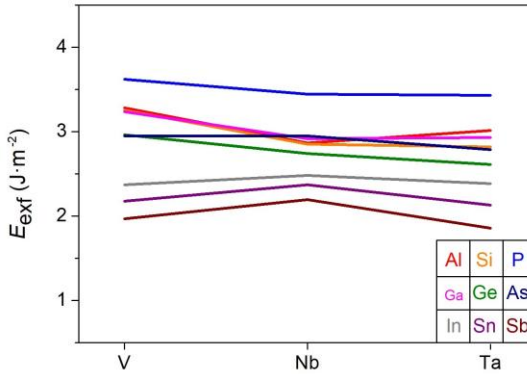


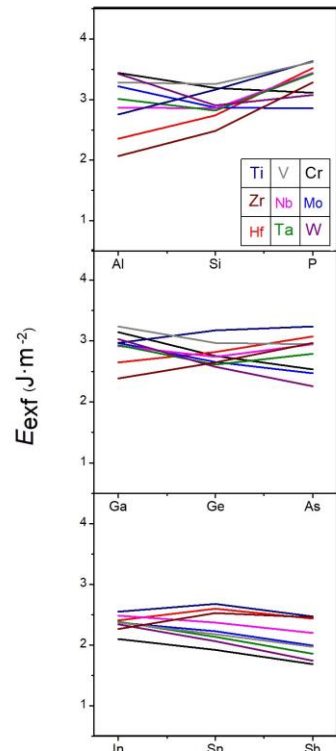
Figure 9:  $E_{\text{exf}}$  variations for V, Nb, and Ta-based  $M_2AC$  phases.

Finally, the last group formed by Cr, Mo, and W is peculiar, see Appendix 2. While Al, Si, P, and Ga show a decrease and later increase in their energies, Ge and As show a decrease in their energies. Sn and Sb show a clear increase and later decrease in their energies, with In having a gradual increase in its energy, with the energy of the Mo derived MAX phase and the W derived MAX phase being very similar.

#### 7.4. EFFECT OF THE P-BLOCK ELEMENT

We start this section discussing the trends along the A element series. The trends along the 3p series with Al, Si, and P are depicted in Figure 10. There, one can see that  $E_{\text{exf}}$  increases for Group IV M metals but decreases for Group VI metals. Finally,  $E_{\text{exf}}$  values decrease moving from Al to Si, but they increase moving towards P for group V metals. Similar trends are captured along the 4p Ga, Ge, and As series. and In, Sn, and Sb-based  $M_2AC$  phases (bottom panel).

Figure 10:  $E_{\text{exf}}$  variations of Al, Si, and P-based  $M_2AC$  phases (top panel), Ga, Ge, and As-based  $M_2AC$  phases (middle panel), and In, Sn, and Sb-based  $M_2AC$  phases (bottom panel)



Lastly, along the 5p In, Sn, Sb series, some changes are found. Whereas the trend for Group VI metals is kept, Group V metals show a decreasing trend, and when have an up-and-down change for Group IV metals, see Figure 10.

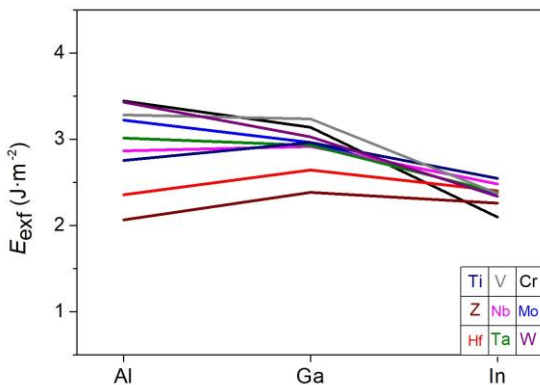


Figure 11:  $E_{\text{exf}}$  variations of Al, Ga, and In-based  $M_2AC$  phases

Continuing the discussion, we shall now focus on the variation along groups within the  $p$ -block. Starting with Al, Ga, and In, see Figure 11,  $E_{\text{exf}}$  is found to increase its value before decreasing, while for the rest, it seems to show a decreasing trend going down the groups. These trends are also observed for the Si, Ge, and Sn group, see Appendix 2. However, the elements of the last row, P, As, and Sb, show a clear trend towards the decrease of these exfoliation energies, see Figure 12.

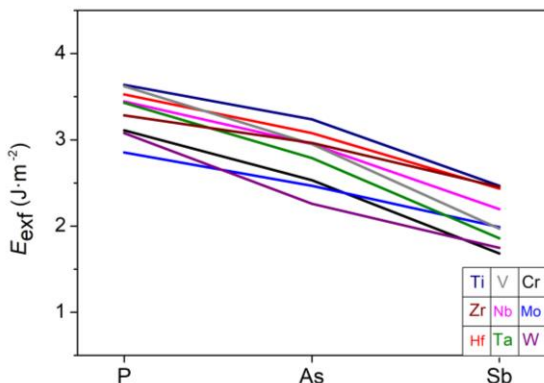


Figure 12:  $E_{\text{exf}}$  variations of P, As, and Sb-based  $M_2AC$  phases

These found trends are roughly the same in carbides and nitrides and independent from the thickness of the phases. There are, however, some exceptions. As an example, in  $M_4AN_3$  phases, in the 3p group of Al, Si, P, instead of the previously described trend, one observes a decrease in energies when going from Al to Si, accompanied by an increase when moving from Si to P.

Finally, to evaluate the difference between nitrides and carbides, we compared the exfoliation energies of both set of data in Figure 13. Overall, the MAC phases feature larger exfoliation energies, compared to MAN phases, although the correlation reveals that both sets of MXenes follow the same trends in general terms.

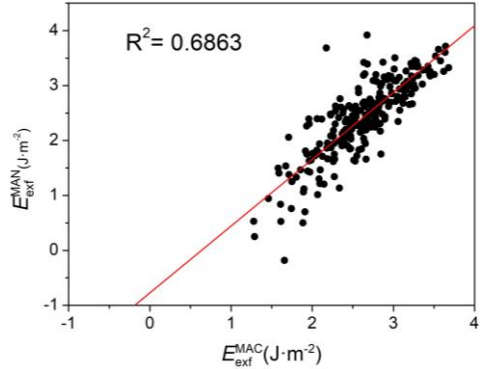


Figure 13: Correlation between MAC and MAN phases  $E_{ext}$ .

## 7.5. WIDTH EFFECT

MXene thickness is a structural factor that slightly influences the adsorption of  $CO_2$ ,<sup>41</sup> as earlier found. Consistently, the variation of  $E_{ext}$  is relatively small as shown in Figure 14. The trends found for a metal seem to be consistent for the different p-block elements. As thickness increases,  $E_{ext}$  for Cr, Mo, and Nb decreases, while for Hf and Zr it increases. Ta shows a peak in its energy when thickness is of 5 layers. On the contrary, W, V and Ti, show the smallest energy when the thickness is of 5 layers.

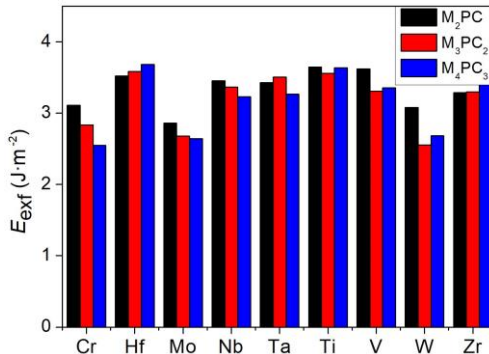


Figure 14: Bar graph with the three studied thicknesses of P-based C-based MAX phases represented.

There are exceptions to this trend. In Figure 15 one can see that the exfoliation energy for Hf decreases with thickness, contrary to the rest of the cases. This is, however, an isolated case, and only happens in this particular case; therefore, it should be considered an exception. The behavior of Zr is also modified in this graph. This can potentially mean that when using Al as the  $p$ -block element, the behavior of such Group IV metals is modified, yet this is not the case for Ti.

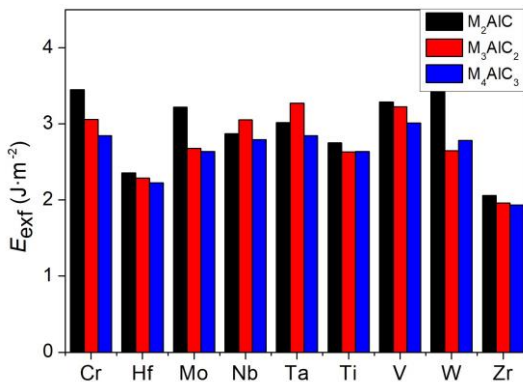


Figure 15: Bar graph with the three studied thicknesses of Al-based C-based MAX phases represented.

## 7.6. BOND DISTANCE M-A EFFECT

The distance between the metal and the  $p$ -block element could be a factor when studying  $E_{\text{exf}}$  of the different phases. As the main difference between the MXene and the MAX precursor is the exfoliation of this  $p$ -block element, it is not a stretch to think that the smaller the distance between the metal and this element, the stronger the bond would be, and, therefore, the harder to exfoliate, and *vice versa*.

As it can be seen in Figure 16, this argument is not fully clear. Al, Si, and Ge are the only  $p$ -metals that clearly show this trend, while for the rest either no correlation at all is observed, such as As, or Ga, or the opposite trend is found, like P, In, Sn, and Sb. Putting aside that metal radii obviously have an impact in the M-A distance, still an analysis by metals can still be done in the ones that do not seem to provide the expected results. First, it can be seen that Zr and Hf appear at values of bond distances larger than the rest and grouped. When comparing the two, a decrease in bond distance when increasing  $E_{\text{exf}}$  can be found, with the sole exception of Sb.

Moreover, following along the supposed trend of these two metals we can find Ti. Another group that behaves similarly is Cr, Mo, and W, and follow the same trend shown with the exception of In, Sn and Sb. Being this the case, it is expected that for V, Nb, and Ta the same trends apply, and indeed they do, with the exception of In, Sn, and Sb. These trends are found to be the same independently of the phases being carbides or nitrides.

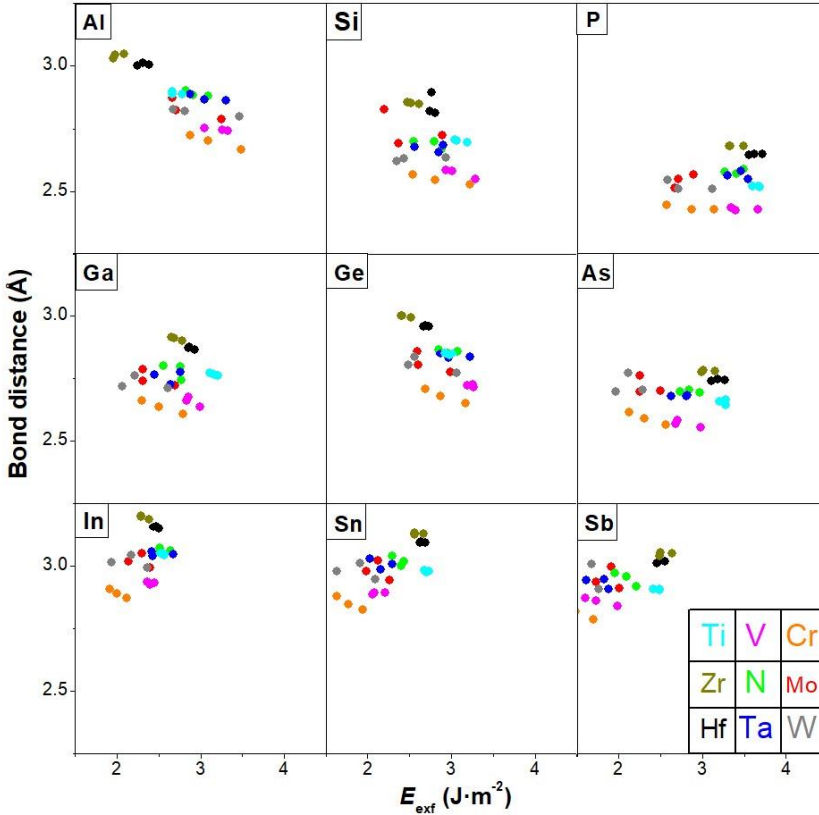


Figure 16: Bond energies of carbide MAC phases in  $p$ -block element order against  $E_{\text{ext}}$ .

## 8. CONCLUSIONS

After studying the exfoliation energy on the different MAX phases, the following conclusions can be extracted:

- Our simulations are consistent with the reference data set of a previous study obtaining very small differences between them.
- There is a partial correlation found between  $E_{\text{ads}}$  of CO<sub>2</sub> and  $E_{\text{exf}}$ , as when the latter increases, the stronger is the adsorption.
- The  $p$ -block element does affect the exfoliation energy. Generally, as one goes down a group in the periodic table, less exfoliating energy is needed to create the MXenes, with the exception of Ti, Zr, and Hf. Along the period, however, it largely depends on the metal.
- Early transition metal does also influence the exfoliation energy. Typically, Ti, Zr, and Hf-derived MAX phases show the smaller exfoliation energy for the greatest found CO<sub>2</sub> adsorption energy. For the rest, group VI show smaller  $E_{\text{ads}}$  in relation with  $E_{\text{exf}}$ , followed by group V.
- Carbide and nitride MAX phases show very similar, almost identical trends, but exfoliation energy of nitride phases is generally smaller than carbide phases.
- The variation of  $E_{\text{exf}}$  due to its width is relatively small. Different early transition metals provide different maximum  $E_{\text{exf}}$  for the different thicknesses.
- M-A bond distances in MAX phases does affect  $E_{\text{exf}}$ . While the general trend is that the larger the distance, the smaller the  $E_{\text{exf}}$ , it truly depends on the metal, where In, Sn and Sb phases are an exception, while the opposite trend can be found, possibly due to them being in the same period.





## 9. REFERENCES AND NOTES

1. Rockström, J., Steffen, W., Noone, K., Persson, Å., Chapin, III, F.S., Lambin, E., Lenton, T.M., Scheffer, M., Folke, C., Schellnhuber, H., Nykvist, B., De Wit, C.A., Hughes, T., van der Leeuw, S., Rodhe, H., Sörlin, S., Snyder, P.K., Costanza, R., Svedin, U., Falkenmark, M., Karlberg, L., Corell, R.W., Fabry, V.J., Hansen, J., Walker, B.H., Liverman, D., Richardson, K., Crutzen, C., Foley, J. A Safe Operating Space for Humanity. *Nature* **2009**, *461*, 472-475.
2. Obama, B. The Irreversible Momentum of Clean Energy. *Science* **2017**, *355*, 126-129.
3. Leung, D. Y. C.; Caramanna, G.; Maroto-Valer, M. M. An Overview of Current Status of Carbon Dioxide Capture and Storage Technologies. *Renew. Sustain. Energy Rev.* **2014**, *39*, 426-443.
4. Gibbins, J.; Chalmers, H. Carbon Capture and Storage. *Energy Policy* **2008**, *36*, 4317-4322.
5. Burghaus, U. Surface Science Studies of Carbon Dioxide Chemistry. In *New and Future Developments in Catalysis*; **2013**.
6. Kunkel, C.; Viñes, F.; Illas, F. Transition Metal Carbides as Novel Materials for CO<sub>2</sub> Capture, Storage, and Activation. *Energy Environ. Sci.* **2016**, *9*, 141-144.
7. Morales-García, Á.; Fernández-Fernández, A.; Viñes, F.; Illas, F. CO<sub>2</sub> Abatement Using Two-Dimensional MXene Carbides. *J. Mater. Chem. A* **2018**, *6*, 3381-3385.
8. Morales-Salvador, R.; Morales-García, Á.; Viñes, F.; Illas, F. Two-Dimensional Nitrides as Highly Efficient Potential Candidates for CO<sub>2</sub> Capture and Activation. *Phys. Chem. Chem. Phys.* **2018**, *20*, 17117-17124.
9. Naguib, M.; Kurtoglu, M.; Presser, V.; Lu, J.; Niu, J.; Heon, M.; Hultman, L.; Gogotsi, Y.; Barsoum, M. W. Two-Dimensional Nanocrystals: Two-Dimensional Nanocrystals Produced by Exfoliation of Ti<sub>3</sub>AlC<sub>2</sub>. *Adv. Mater.* **2011**, *23*, 4248-4253.
10. Li, T.; Yao, L.; Liu, Q.; Gu, J.; Luo, R.; Li, J.; Yan, X.; Wang, W.; Liu, P.; Chen, B.; et al. Fluorine-Free Synthesis of High-Purity Ti<sub>3</sub>C<sub>2</sub>T<sub>x</sub> (T=OH, O) via Alkali Treatment. *Angew. Chem. Int. Ed.* **2018**, *57*, 6115-6119.
11. Khazaei, M.; Ranjbar, A.; Esfarjani, K.; Bogdanovski, D.; Dronskowski, R.; Yunoki, S. Insights into Exfoliation Possibility of MAX Phases to MXenes. *Phys. Chem. Chem. Phys.* **2018**, *20*, 8579-8592.
12. Urbankowski, P.; Anasori, B.; Makaryan, T.; Er, D.; Kota, S.; Walsh, P. L.; Zhao, M.; Shenoy, V. B.; Barsoum, M. W.; Gogotsi, Y. Synthesis of Two-Dimensional Titanium Nitride Ti<sub>4</sub>N<sub>3</sub> (MXene). *Nanoscale* **2016**, *8*, 11385-11391.
13. Shahid, S.; Billington, R. W.; Hill, R. G. The Effect of Ultrasound on the Uptake of Fluoride by Glass Ionomer Cements. *J. Mater. Sci. Mater. Med.* **2011**, *22*, 247-251.
14. Schrödinger, E. An Undulatory Theory of the Mechanics of Atoms and Molecules. *Phys. Rev.* **1928**, *28*, 1049-1070.
15. Born, M.; Oppenheimer, R. Zur Quantentheorie Der Molekeln. *Ann. Phys.* **1927**, *389*, 457-484.
16. Hartree, D. R. The Wave Mechanics of an Atom with a Non-Coulomb Central Field Part I Theory and Methods. *Math. Proc. Cambridge Philos. Soc.* **1928**, *24*, 89-110.
17. Hohenberg, P.; Kohn, W. Inhomogeneous Electron Gas. *Phys. Rev.* **1964**, *136*, 864-871.
18. Thomas, L. H. The Calculation of Atomic Fields. *Math. Proc. Cambridge Philos. Soc.* **1927**, *23*, 542-548.

19. Fermi, E. Statistical Method to Determine Some Properties of Atoms. *Rend. Accad. Naz. Lincei* **1927**, *6*, 602-607.
20. Feynman, R. P.; Cohen, M. Energy Spectrum of the Excitations in Liquid Helium Appendix A. *Phys. Rev.* **1956**, *102*, 1189-1204.
21. Seminario, J. M. An Introduction to Density Functional Theory in Chemistry. *Theor. Comput. Chem.* **1995**, *2*, 1-27.
22. Kohn, W.; Sham, L. J. Self-Consistent Equations Including Exchange and Correlation Effects. *Phys. Rev.* **1965**, *140*, A1133-A1138.
23. Burke, K.; Wagner, L. O. DFT in a Nutshell. *Int. J. Quantum Chem.* **2013**, *113*, 96-101.
24. Borlido, P.; Aull, T.; Huran, A. W.; Tran, F.; Marques, M. A. L.; Botti, S. Large-Scale Benchmark of Exchange-Correlation Functionals for the Determination of Electronic Band Gaps of Solids. *J. Chem. Theory Comput.* **2019**, *15*, 5069-5079.
25. Bagayoko, D. Understanding Density Functional Theory (DFT) and Completing It in Practice. *AIP Adv.* **2014**, *4*, 127104.
26. Perdew, J. P.; Chevary, J. A.; Vosko, S. H.; Jackson, K. A.; Pederson, M. R.; Singh, D. J.; Fiolhais, C. Atoms, Molecules, Solids, and Surfaces: Applications of the Generalized Gradient Approximation for Exchange and Correlation. *Phys. Rev. B* **1992**, *46*, 6671-6687.
27. Hohenstein, E. G.; Chill, S. T.; Sherrill, C. D. Assessment of the Performance of the M05 and M06 Exchange Correlation Functionals for Noncovalent Interactions in Biomolecules. *J. Chem. Theory Comput.* **2008**, *4*, 1996-2000.
28. Laue, M. Von. Concerning the Detection of X-Ray Interferences. *Nobel Lect.* **1915**.
29. Bloch, F. Über Die Quantenmechanik Der Elektronen in Kristallgittern (About the Quantum Mechanics of Electrons in Crystal Lattices). *Zeitschrift für Phys.* **1928**, *52*, 555-600.
30. Huff, W. D. X-Ray Diffraction and the Identification and Analysis of Clay Minerals. *Clays Clay Miner.* **1990**, *38*, 448.
31. Jeitschko, W.; Nowotny, H.; Benesovsky, F. Ti<sub>2</sub>AlN, Eine Stickstoffhaltige H-Phase. *Monatshefte für Chemie* **1963**, *94*, 1198-1200.
32. Deysher G, Shuck CE, Hantanasirisakul K, et al. Synthesis of Mo<sub>4</sub>VAIC<sub>4</sub> MAX Phase and Two-Dimensional Mo<sub>4</sub>VC<sub>4</sub> MXene with Five Atomic Layers of Transition Metals. *ACS Nano.* **2020**, *14* (1), 204-217.
33. Gogotsi, Y. Transition Metal Carbides Go 2D. *Nat. Mater.* **2015**, *14*, 1079-1080.
34. Xu, C.; Wang, L.; Liu, Z.; Chen, L.; Guo, J.; Kang, N.; Ma, X. L.; Cheng, H. M.; Ren, W. Large-Area High-Quality 2D Ultrathin Mo<sub>2</sub>C Superconducting Crystals. *Nat. Mater.* **2015**, *14*, 1135-1141.
35. Jung, J. H.; Park, C. H.; Ihm, J. A Rigorous Method of Calculating Exfoliation Energies from First Principles. *Nano Lett.* **2018**, *18*, 2759-2765.
36. Perdew, J. P.; Burke, K.; Ernzerhof, M. Generalized Gradient Approximation Made Simple. *Phys. Rev. Lett.* **1996**, *77*, 3865-3868.
37. Kresse, G.; Furthmüller, J. Efficient Iterative Schemes for Ab Initio Total-Energy Calculations Using a Plane-Wave Basis Set. *Phys. Rev. B - Condens. Matter Mater. Phys.* **1996**, *54*, 11169-11186.
38. Blöchl, P. E. Projector Augmented-Wave Method. *Phys. Rev. B* **1994**, *50*, 17953-17979.
39. Monkhorst, H. J.; Pack, J. D. Special Points for Brillouin-Zone Integrations. *Phys. Rev. B* **1976**, *13*, 5188-5192.
40. Horlait, D.; Grasso, S.; Chroneos, A.; Lee, W. E. Attempts to Synthesize Quaternary MAX Phases (Zr,m)<sub>2</sub>ALC and Zr<sub>2</sub>(AL,A)C as a Way to Approach Zr<sub>2</sub>ALC. *Mater. Res. Lett.* **2016**, *4*, 137-144.
41. Morales-García, Á.; Mayans-Llorach, M.; Viñes, F.; Illas, F. Thickness Biased Capture of CO<sub>2</sub> on Carbide MXenes. *Phys. Chem. Chem. Phys.* **2019**, *21*, 23136-23142.

# APPENDICES



## APPENDIX 1: TABLES

		$E_{\text{exf}} \text{M}_3\text{AX}_2 \text{ (J}\cdot\text{m}^{-2}\text{)}$									
<b>X</b>	<b>MA</b>	<b>Al</b>	<b>Si</b>	<b>P</b>	<b>Ga</b>	<b>Ge</b>	<b>As</b>	<b>In</b>	<b>Sn</b>	<b>Sb</b>	
<b>C</b>	<b>d<sup>2</sup></b>	<b>Ti</b>	2.63	3.01	3.56	2.88	3.08	3.17	2.50	2.64	2.39
		<b>Zr</b>	1.96	2.45	3.30	2.37	2.63	2.98	2.26	2.53	2.47
		<b>Hf</b>	2.29	2.71	3.59	2.66	2.84	3.14	2.44	2.61	2.47
	<b>d<sup>3</sup></b>	<b>V</b>	3.22	2.98	3.30	3.16	2.80	2.68	2.34	2.04	1.71
		<b>Nb</b>	3.04	2.77	3.37	3.04	2.72	2.80	2.61	2.40	2.07
		<b>Ta</b>	3.27	2.87	3.51	3.19	2.72	2.77	2.64	2.26	1.81
	<b>d<sup>4</sup></b>	<b>Cr</b>	3.06	2.77	2.84	2.84	2.47	2.28	1.97	1.75	1.46
		<b>Mo</b>	2.68	2.18	2.68	2.56	2.29	2.23	2.12	1.97	1.71
		<b>W</b>	2.64	2.32	2.55	2.45	2.04	1.94	1.91	1.62	1.30
<b>N</b>	<b>d<sup>2</sup></b>	<b>Ti</b>	3.19	3.30	3.65	3.16	3.14	3.03	2.45	2.37	2.00
		<b>Zr</b>	2.39	2.63	3.37	2.50	2.68	2.87	2.08	2.32	2.08
		<b>Hf</b>	2.63	2.76	3.45	2.64	2.71	2.79	2.10	2.23	1.84
	<b>d<sup>3</sup></b>	<b>V</b>	3.17	2.85	3.19	2.95	2.56	2.45	1.99	1.71	1.38
		<b>Nb</b>	2.80	2.60	3.28	2.72	2.48	2.69	2.18	2.05	1.79
		<b>Ta</b>	2.95	2.48	3.20	2.66	2.24	2.40	1.97	1.68	1.33
	<b>d<sup>4</sup></b>	<b>Cr</b>	2.34	2.24	2.31	2.16	1.84	1.67	1.43	1.25	0.95
		<b>Mo</b>	3.40	3.69	3.93	2.87	2.53	2.47	2.39	2.31	2.07
		<b>W</b>	3.22	2.42	2.52	2.63	1.75	1.44	0.71	0.53	0.26

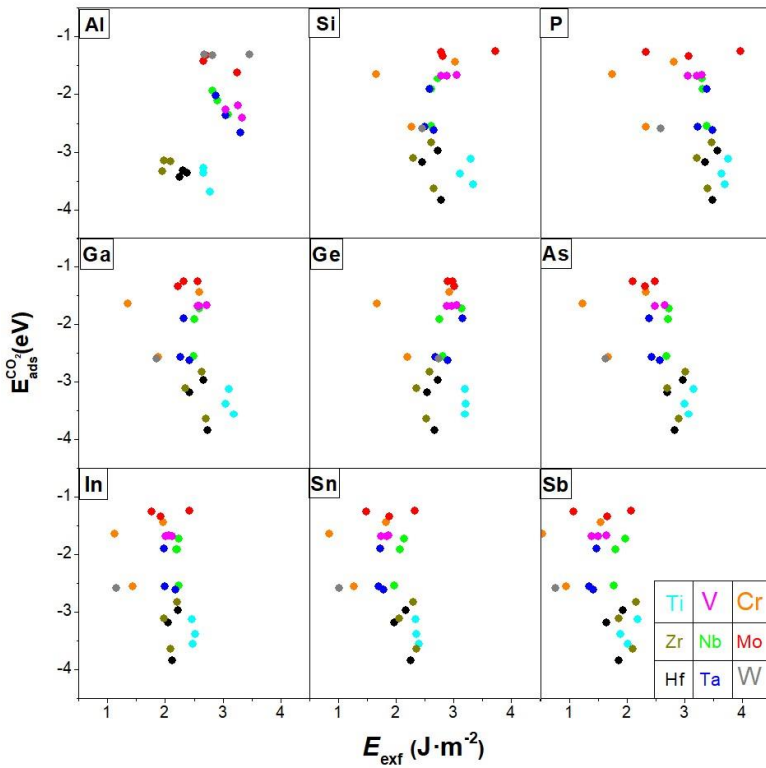
Table 2: Exfoliation energies for carbide and nitride obtained from M<sub>3</sub>AX<sub>2</sub> phases.

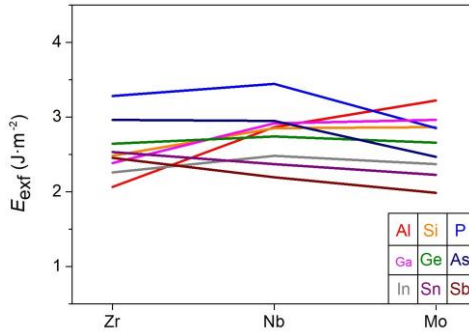
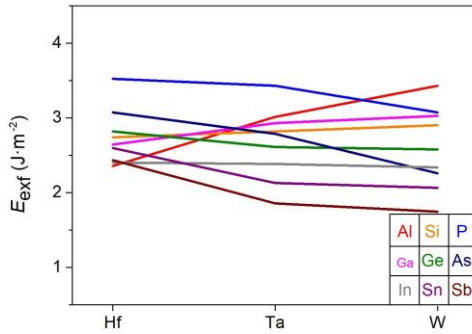
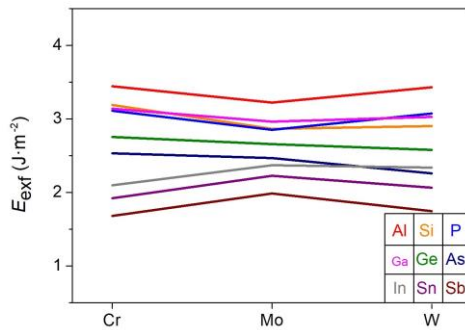
		$E_{\text{exf}} \text{M}_4\text{AX}_3 \text{ (J}\cdot\text{m}^{-2}\text{)}$									
<b>X</b>	<b>M/A</b>	<b>Al</b>	<b>Si</b>	<b>P</b>	<b>Ga</b>	<b>Ge</b>	<b>As</b>	<b>In</b>	<b>Sn</b>	<b>Sb</b>	
<b>C</b>	$d^2$	<b>Ti</b>	2.64	3.03	3.64	2.95	3.12	3.24	2.53	2.71	2.45
		<b>Zr</b>	1.94	2.58	3.46	2.48	2.76	3.12	2.36	2.63	2.61
		<b>Hf</b>	2.23	2.79	3.69	2.71	2.90	3.24	2.48	2.66	2.53
	$d^3$	<b>V</b>	3.01	2.90	3.37	3.22	2.82	2.66	2.42	2.05	1.59
		<b>Nb</b>	2.79	2.53	3.24	2.82	2.53	2.71	2.48	2.28	1.94
		<b>Ta</b>	2.84	2.53	3.27	2.84	2.42	2.60	2.39	2.00	1.59
	$d^4$	<b>Cr</b>	2.84	2.52	2.55	2.66	2.28	2.10	1.91	1.60	1.28
		<b>Mo</b>	2.64	2.34	2.64	2.56	2.29	2.23	2.28	2.10	1.89
		<b>W</b>	2.79	2.40	2.68	2.53	2.20	2.08	2.15	1.89	1.67
<b>N</b>	$d^2$	<b>Ti</b>	3.19	3.08	3.61	3.19	3.01	2.96	2.50	2.32	1.88
		<b>Zr</b>	2.26	2.26	3.17	2.32	2.32	2.68	1.97	2.04	1.84
		<b>Hf</b>	2.48	2.42	3.32	2.52	2.39	2.66	2.04	1.94	1.63
	$d^3$	<b>V</b>	3.09	2.76	3.03	2.85	2.53	2.47	2.10	1.83	1.49
		<b>Nb</b>	3.08	2.60	3.35	2.79	2.45	2.66	2.21	1.94	1.75
		<b>Ta</b>	2.98	2.63	3.46	2.87	2.39	2.55	2.16	1.76	1.41
	$d^4$	<b>Cr</b>	1.75	1.63	1.71	1.67	1.35	1.22	1.12	0.83	0.53
		<b>Mo</b>	3.43	2.76	2.31	2.95	2.29	2.08	1.75	1.47	1.06
		<b>W</b>	3.20	2.34	2.39	2.56	1.67	1.30	1.20	0.50	-0.18

Table 3: Exfoliation energies for carbide and nitride obtained from  $\text{M}_4\text{AX}_3$  phases

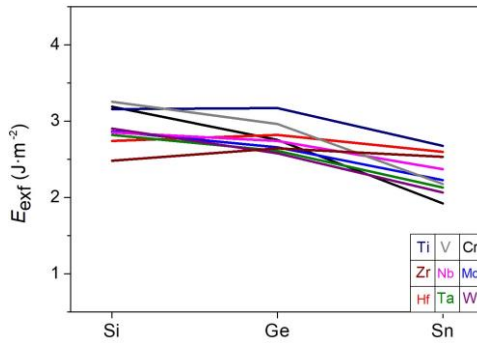
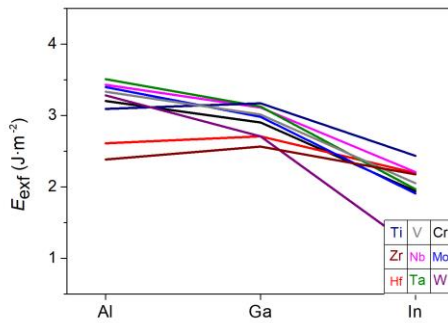
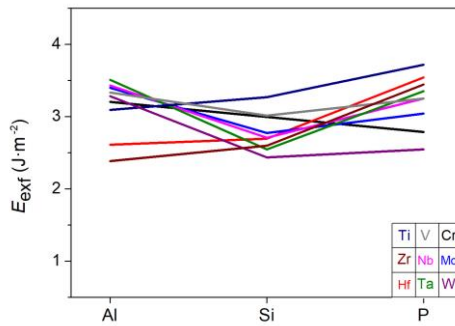
:

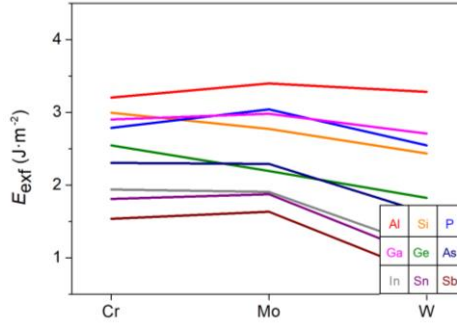
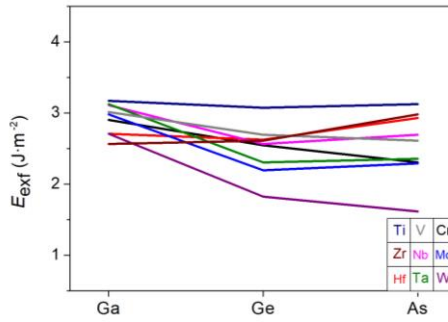
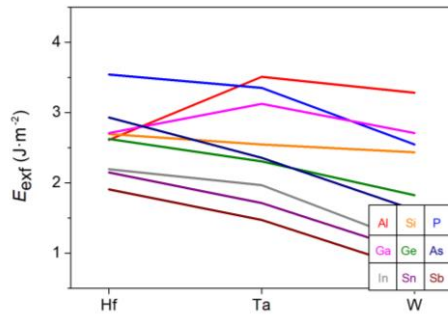
## APPENDIX 2: GRAPHS

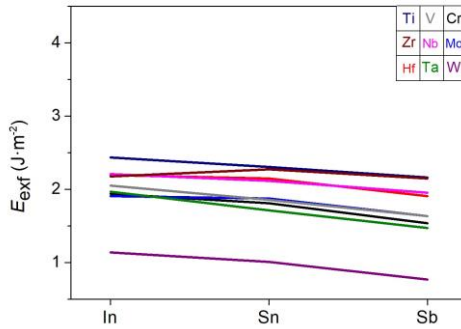
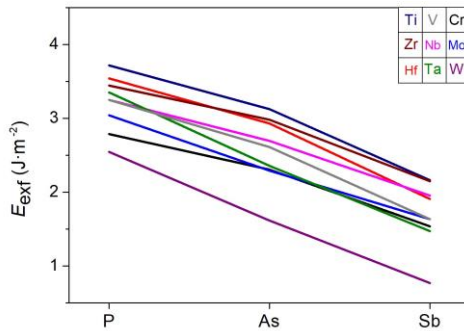
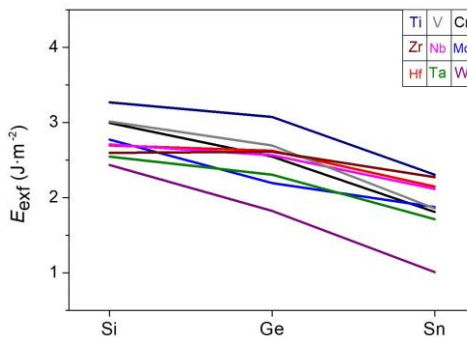
Figure 17:  $E_{\text{ext}}$  for nitride  $M_{n+1}AX_n$  ( $n=1,2,3$ ) phases.

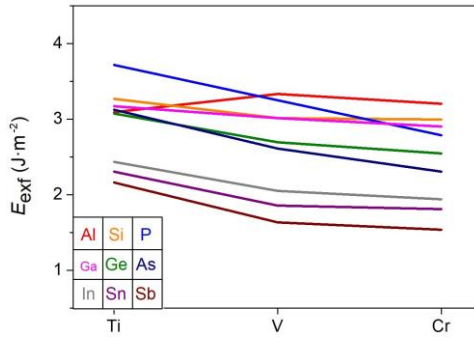
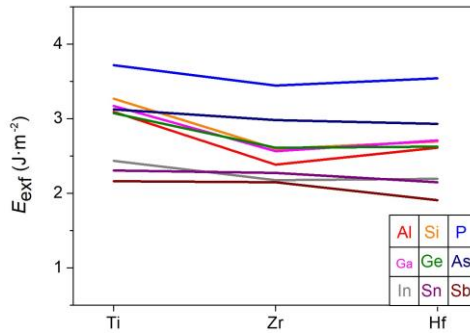
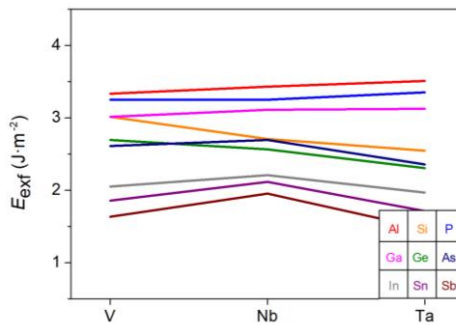
Figure 18:  $E_{\text{exf}}$  variations for Zr, Nb, and Mo-based  $M_2AC$  phases.Figure 19:  $E_{\text{exf}}$  variations for Hf, Ta, and W-based  $M_2AC$  phases.Figure 20:  $E_{\text{exf}}$  variations for Cr, Mo, and W-based  $M_2AC$  phases.

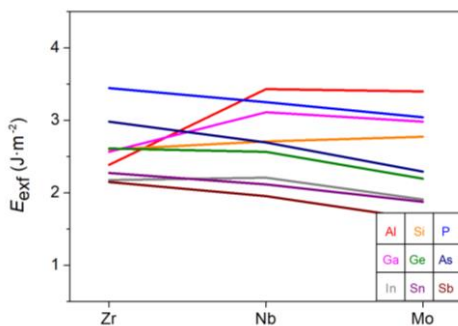
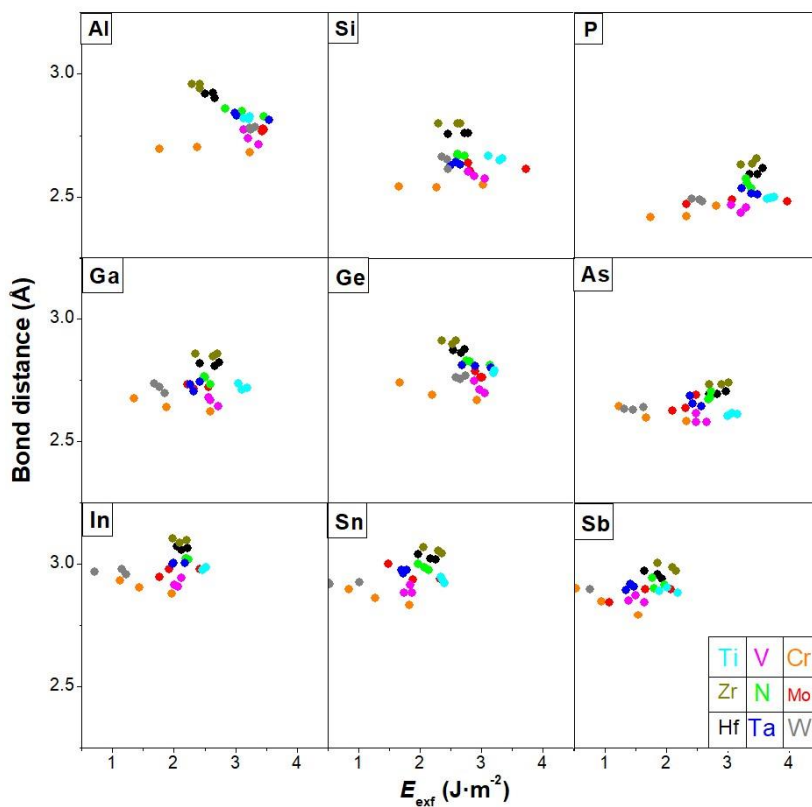


Figure 21:  $E_{\text{exf}}$  variations for Si, Ge, and Sn-based M<sub>2</sub>AC phases.Figure 22:  $E_{\text{exf}}$  variations for Al, Ga, and In-based M<sub>2</sub>AN phases.Figure 23:  $E_{\text{exf}}$  variations for Al, Si, and P-based M<sub>2</sub>AN phases.

Figure 24:  $E_{\text{exf}}$  variations for Cr, Mo, and W-based  $M_2AN$  phasesFigure 25:  $E_{\text{exf}}$  variations for Ga, Ge, and As-based  $M_2AN$  phases.Figure 26:  $E_{\text{exf}}$  variations for Hf, Ta, and W-based  $M_2AN$  phases.

Figure 27:  $E_{\text{exf}}$  variations for In, Sn, and Sb-based M<sub>2</sub>AN phase.Figure 28:  $E_{\text{exf}}$  variations for P, As, and Sb-based M<sub>2</sub>AN phases.Figure 29:  $E_{\text{exf}}$  variations for Si, Ge, and Sn-based M<sub>2</sub>AN phases.

Figure 30:  $E_{\text{exf}}$  variations for Ti, V, and Cr-based  $M_2AN$  phase.Figure 31:  $E_{\text{exf}}$  variations for Ti, Zr, and Hf-based  $M_2AN$  phases.Figure 32:  $E_{\text{exf}}$  variations for V, Nb, and Ta-based  $M_2AN$  phases.

Figure 33:  $E_{\text{exf}}$  variations for Zr, Nb, and Mo-based  $M_2AN$  phases.Figure 34: Bond energies of carbide MAC phases in  $p$ -block element order against  $E_{\text{exf}}$ .



